# Estimering av ytelsesparametre for en skihopper uten bruk av merking ved punkt og linjeskjæring

Atle Nes, Ingolf Hådem og Jan H. Nilsen

Vitenskapelig bedømt (refereed) artikkel

*Atle Nes et al.: Markerless estimation of performance parameters of a ski jumper using point and line intersection*

KART OG PLAN, Vol. 76, pp. 305–318, POB 5003, NO-1432 Ås, ISSN 0047-3278.

Ski jumping analysis belongs to the domain of human motion analysis with focus on (i) the construction of an object model and (ii) markerless estimation not always based on optimal least squares (Poppe, 2007). (Schwameder, et al., 2005) and (Virmavirta, et al., 2005) study characteristics of the early flight phase, and (Schwameder, 2008) does biomechanical research on ski jumping. (Nes, et al., 2012) estimate early flight performance in a real case, using markers on the body/skis, called a "marker-based" approach. In the present article we study theoretical and practical consequences of applying the markerless approach to optimal estimation of performance parameters and their precision. Assuming body/skis are modelled as straight lines, the present article describes 2D measurement of freely chosen image line points and the formulas for computing corresponding 3D body/ski lines by **line intersection** (with "error free" camera poses). The present article uses a fairly new method for deriving formulae for a one-step optimal line intersection and the estimated line accuracy. The article also shows the derivation of formulas for computing the "inner" and "outer" performance parameters and body/ski model position and ski separation. A simulated example is included, which demonstrates ill-conditioned problems encountered by line intersection.

*Keywords:* markerless line photogrammetry, performance of ski jumper

*Atle Nes*, Assistant Professor, Department of Informatics and e-Learning Faculty of Technology, NTNU, POB 8900, NO-7491 Trondheim. E-mail: atle.nes@ntnu.no

## 1 Introduction

### *1.1 Goal and tasks*

The goal of this article is to study theoretical and practical aspects of applying markerless line photogrammetry to track and analyze the performance of a ski jumper in flight using synchronous images acquired by stationary video cameras. The paper is divided into 4 sections addressing the following tasks. Section 2: Defining actual performance parameters using a geometric line model of body/skis. Section 3: Defining the methods of image measurement and computation of performance parameters. Section 4: Presenting a simulated example of computing three "inner" performance parameters in a stereo pair situation. Section 5: Summarizing and commenting on the work, and proposing further tasks.

### *1.2 Previous work*

Markerless analysis of the performance of a ski jumper belongs to the domain of human motion analysis. (Poppe, 2007) gives an overview of the activities, focusing on different approaches to segmentation and segment estimation. (Schwameder, et al., 2005) and (Virmavirta, et al., 2005) study characteristics of the early flight phase, and (Schwameder, 2008) Schwameder (2008) does biomechanical research in ski jumping. The present article is related to (Nes, et al., 2012) who report on a real case of applying photogrammetric tracking and analyzing 3D motion of a ski jumper over a 20 m flight phase in Granåsen ski jumping hill, where images are acquired by a triplet of stationary video cameras. Reflective markers on the jump suit, helmet and skis serve as targets that are identified and intersected in the field coordi-

nate system to estimate performance parameters like position, speed, Boklöv angle and upper- and lower body closing angles (Ryu, et al., 2015; Jung, et al., 2015). Accuracies are derived by the Monte Carlo method (Hastedt, 2004).

## 2 Geometry of the body/ski model and its performance parameters

This section presents a geometric stick model of body/skis (Fig. 2) and the camera (Fig. 1). Here we give an overview of notations with explanation of composed geometric elements as 2D and 3D points and lines (Section 2.1–2.3), introduce the concepts of "outer" and "inner" performance parameters (Section 2.5), and build collinearity equations of points (Section 2.4) and lines (Section 2.6).

### *2.1 Symbols of relevant points and lines with explanation*

Euclidean vectors in ***bold italic***, homogenous vectors in **bold regular**

$\boldsymbol{x} = [x, y]^{\mathrm{T}}$ **Euclid** coordinate vector of a **2D point**

$\boldsymbol{X} = [X, Y, Z]^{\mathrm{T}}$ **Euclid** coordinate vector of a **3D point**

$\mathbf{x} = \begin{bmatrix} \boldsymbol{x}_0 \\ x_{\mathrm{h}} \end{bmatrix} = \begin{bmatrix} x_1 \\ x_2 \\ — \\ x_3 \end{bmatrix}$ **Homogenous** coordinate vector of a **2D point** (chapter 2.3.1.2.1 in (McGlone, 2004), p. 113). Subscript "0" indicates the Euclid part and "h" indicates the homogenous part. Dividing by $x_{\mathrm{h}}$ gives $\mathbf{x} = [x, y, 1]^{\mathrm{T}}$.

$\mathbf{l} = \begin{bmatrix} \boldsymbol{l}_0 \\ l_{\mathrm{h}} \end{bmatrix} = \begin{bmatrix} l_1 \\ l_2 \\ — \\ l_3 \end{bmatrix}$ **Homogenous** vector of a 2D line (chapter 2.3.1.2.2 in (McGlone, 2004), p. 114). Introducing $[l_1, l_2, l_3]^{\mathrm{T}} \equiv [a, -1, b]^{\mathrm{T}}$ the 2D line equation becomes $[l_1, l_2, l_3][x, y, 1]^{\mathrm{T}} = 0$ or in short $\mathbf{l}^{\mathrm{T}}\mathbf{x} = 0$.

$\boldsymbol{q} = [\alpha, \beta, \gamma, \delta]^{\mathrm{T}}$ **Euclid** parameter vector of a **3D line** (section 4.5.2 in (Luhmann, et al., 2006), p. 296) where $\alpha, \gamma$ are the direction and position parameters of the projection line in the XZ-plane and $\beta, \delta$ are the corresponding parameters of the projection line in the XY-plane (Fig. 3-B).

### *2.2 Number notations*

| | |
|---|---|
| i = 1, .. $n_{im}$ | number of image views or individual cameras |
| j = 1, 2 | number of 3D legs or ski lines |
| k = 1, .. $(n_{leg})_{i,j}$ or $(n_{ski})_{i,j}$ | number of 2D points on leg lines $(l_{leg})_{i,j}$ or on ski lines $(l_{ski})_{i,j}$ |

### *2.3 Point and line notations*

| 3D object points and lines | 2D image points and lines |
|---|---|
| $P_{helm}$ : center of helmet | $(p_{helm})_i$ : corresponding to $P_{helm}$ |
| $(P_{bind})_j$ : corresponding to $(p_{bind})_{i,j}$ | $(p_{bind})_{i,j}$ : intersection of $(l_{leg})_{i,j}$ , $(l_{ski})_{i,j}$ |
| $(L_{leg})_j$ : lines through $P_{helm}$ and $(P_{bind})_j$ | $(l_{leg})_{i,j}$ : corresponding to $(L_{leg})_j$ |
| $(L_{ski})_j$ : straight lines of skies | $(l_{ski})_{i,j}$ : corresponding to $(L_{ski})_j$ |
| No corresponding points | $(p_{leg}$ or $p_{ski})_{i,j,k}$ : point k on 2D line $(l_{leg}$ or $l_{ski})_{i,j}$ |

$L_{mid}$ middle line between the ski lines $(L_{ski})_j$
$P_{mid}$ middle point between points $(P_{bind})_j$ (the position of which may act as the model position)

### *2.4 Collinearity equations*

The general collinear equations with modelled linear and non-linear image errors are given by Eq. (4.8) in (Luhmann, et al., 2006), p. 205). We assume, however, an ideal camera ((McGlone, 2004), p. 230–232) with (i) known principal distance, (ii) known principal point and (iii) camera system translated and rotated in the object system as shown in Fig. 1 and given in Eq. (1).

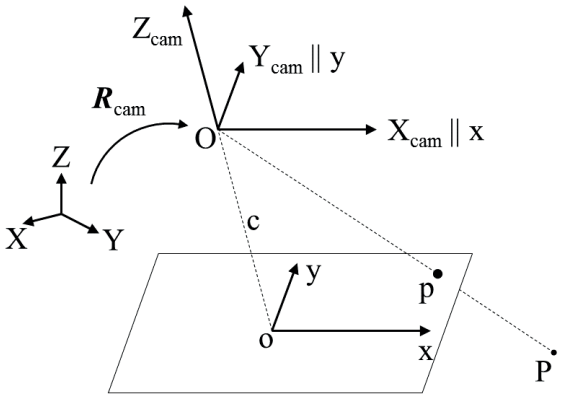


*Figure 1. Geometry of an ideal camera. Projection center (O). Object point (P). Principal distance (c) and principal point (o). Image system (x, y). Object system (X,Y,Z). Camera system* $(X,Y,Z)_{\text{cam}}$*. Rotation* $(\boldsymbol{R}_{\text{cam}})$ *of camera system.*

$$x = -c\frac{\left[\boldsymbol{X}-\boldsymbol{X}_0\right]^{\mathrm{T}}\left(\boldsymbol{r}_1\right)_{\text{cam}}}{\left[\boldsymbol{X}-\boldsymbol{X}_0\right]^{\mathrm{T}}\left(\boldsymbol{r}_3\right)_{\text{cam}}},\quad y = -c\frac{\left[\boldsymbol{X}-\boldsymbol{X}_0\right]^{\mathrm{T}}\left(\boldsymbol{r}_2\right)_{\text{cam}}}{\left[\boldsymbol{X}-\boldsymbol{X}_0\right]^{\mathrm{T}}\left(\boldsymbol{r}_3\right)_{\text{cam}}} \tag{1}$$

with $\boldsymbol{X} = \left[X,Y,Z\right]^{\mathrm{T}}$, $\boldsymbol{X}_0 = \left[X,Y,Z\right]_0^{\mathrm{T}}$. The elements of vectors $\left(\boldsymbol{r}_1,\boldsymbol{r}_2,\boldsymbol{r}_3\right)_{\text{cam}}$ of the rotation matrix $\boldsymbol{R}_{\text{cam}}$ (Eq. (2)) are trigonometric functions of angles $\left(\kappa,\varphi_\kappa,\omega_{\kappa,\varphi}\right)_{\text{cam}}$ rotating about movable axes (conf. Eq. (2.18) in (Luhmann, et al., 2006), p. 40).

$$\left(\boldsymbol{R} = \begin{bmatrix}\boldsymbol{r}_1^{\mathrm{T}}\\ \boldsymbol{r}_2^{\mathrm{T}}\\ \boldsymbol{r}_3^{\mathrm{T}}\end{bmatrix} = \begin{bmatrix}r_{11} & r_{12} & r_{13}\\ r_{21} & r_{22} & r_{23}\\ r_{31} & r_{32} & r_{33}\end{bmatrix}\right)_{\text{cam}} \tag{2}$$

$$= \begin{bmatrix}\cos\varphi_\kappa\cos\kappa & -\cos\varphi_\kappa\sin\kappa & \sin\varphi_\kappa\\ \cos\omega_{\kappa,\varphi}\sin\kappa+\sin\omega_{\kappa,\varphi}\sin\varphi_\kappa\cos\kappa & \cos\omega_{\kappa,\varphi}\cos\kappa-\sin\omega_{\kappa,\varphi}\sin\varphi_\kappa\sin\kappa & -\sin\omega_{\kappa,\varphi}\cos\varphi_\kappa\\ \sin\omega_{\kappa,\varphi}\sin\kappa+\cos\omega_{\kappa,\varphi}\sin\varphi_\kappa\cos\kappa & \sin\omega_{\kappa,\varphi}\cos\kappa+\cos\omega_{\kappa,\varphi}\sin\varphi_\kappa\sin\kappa & \cos\omega_{\kappa,\varphi}\cos\kappa\end{bmatrix}_{\text{cam}}$$

### *2.5 "Outer" and "inner" performance parameters*

*The "outer" parameters* are the angles $\kappa,\varphi_\kappa,\omega_{\kappa,\varphi}$ obtained by stepwise transformations (Eq. (3)). Note that the transformations Eq. (3a) and Eq. (3b) with $L_{\text{mid}}$ are constrained by $(\beta_{\text{mid}})_\kappa = 0$ in the κ-rotated system $\boldsymbol{X}_\kappa$ and $(\alpha_{\text{mid}})_{\kappa\varphi} = 0$ in the κφ-rotated system $\boldsymbol{X}_{\kappa\varphi}$. The transformation Eq. (3c) is constrained by $(Y_{\text{helm}})_{\kappa\varphi\omega} = 0$ in the κφω-rotated system $\boldsymbol{X}_{\kappa\varphi\omega}$. $\boldsymbol{X}_{\kappa\varphi\omega}$ (also denoted $\boldsymbol{X}_{\text{jumper}}$) is the body/ski model system and the elements of $\boldsymbol{R}_{\kappa\varphi\omega}$ (also denoted as $\boldsymbol{R}_{\text{jumper}}$) are trigonometric functions in the rotation angles corresponding to Eq. (2).

**Direction** κ - angle rotation about Z

$$\boldsymbol{X}_{\kappa} = \boldsymbol{R}_{\kappa}\boldsymbol{X}, \quad \left(\beta_{\text{mid}}\right)_{\kappa} = 0 \tag{3a}$$

**Forward slope** $\varphi_{\kappa}$ - angle rotation about $Y_{\kappa}$

$$\boldsymbol{X}_{\kappa\varphi} = \boldsymbol{R}_{\kappa\varphi}\boldsymbol{X}, \quad \left(\alpha_{\text{mid}}\right)_{\kappa\varphi} = 0 \tag{3b}$$

**Sideway slope** $\omega_{\kappa\varphi}$ - angle rotation about $X_{\kappa\varphi}$

$$\boldsymbol{X}_{\kappa\varphi\omega} = \boldsymbol{R}_{\kappa\varphi\omega}\boldsymbol{X}, \quad \left(\text{Y}_{\text{helm}}\right)_{\kappa\varphi\omega} = 0 \tag{3c}$$

*The "inner" parameters* are defined as the angles $(\Psi, \Phi, \Omega)$.
**Boklöv angle** $(\Psi)$is the angle between projected lines $(L_{ski})_j$ in XY-plane. **Scissor angle** $(\Phi)$ is the angle between projected lines $(L_{ski})_j$ in XZ-plane. **Closing angle** $(\Omega)$ is the angle between the line $L_{mid}$ and the line through $P_{helm}$ and $P_{mid}$.

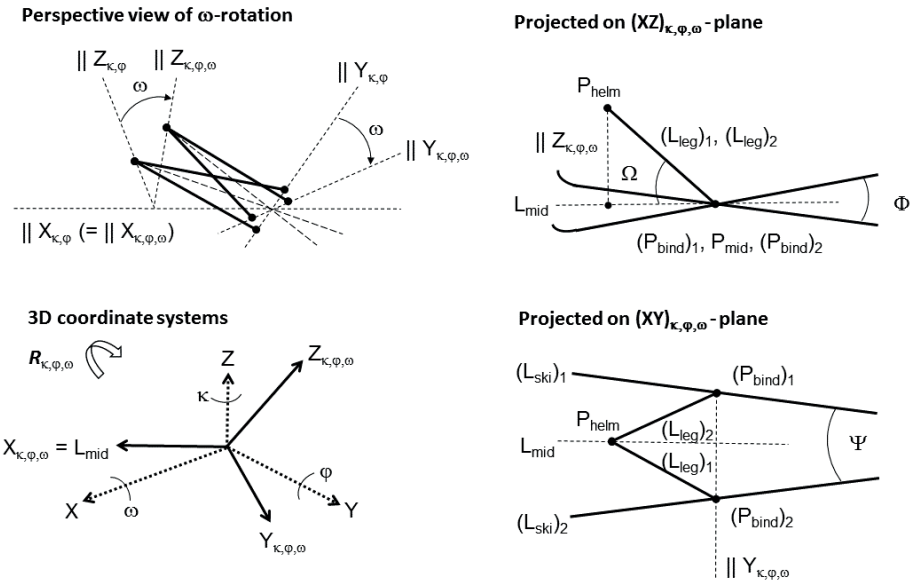


*Figure 2. Model geometry of the ski jumper.* $P_{mid}$ *is the midpoint of* $(P_{bind})_1$ *and* $(P_{bind})_2$.

### *2.6 Collinearity equations of lines*

On the basis of (i) the image line equation in Fig. 3-A, (ii) the corresponding object line equations in Fig. 3-B and (iii) the collinearity equations (Eq. (1)) the collinearity equations of lines are derived as (conf. Eq. (4.130) in (Luhmann, et al., 2006)).

$$\text{a} = \frac{\boldsymbol{u}^{\text{T}}\boldsymbol{r}_1}{-\boldsymbol{u}^{\text{T}}\boldsymbol{r}_2}, \quad \text{b} = -\text{c}\frac{\boldsymbol{u}^{\text{T}}\boldsymbol{r}_3}{-\boldsymbol{u}^{\text{T}}\boldsymbol{r}_2} \tag{4a}$$

$$\boldsymbol{u} = \left[\tau - \alpha\text{Y}_0 + \beta\text{Z}_0, \quad \alpha\text{X}_0 + \gamma - \text{Z}_0, \quad -\left(\beta\text{X}_0 + \delta - \text{Y}_0\right)\right]^{\text{T}} \tag{4b}$$

$$\tau = \alpha\delta - \beta\gamma \tag{4c}$$

## 3 Image measurement and computation of performance parameters

Section 3.1 gives the main steps and algorithms, with references to the present article and the literature. Section 3.2 formulates spatial intersections of points and lines. Section 3.3 formulates rotational transformation of lines. Section 3.4 builds equation systems to solve and compute actual performance parameters and their precision.

### *3.1 Procedure of estimating the performance*

*Main steps*

2D operations:
- Measure helmet point and random ski line points.
- Compute ski binding points as the intersection between skies and corresponding leg lines.

3D operations:
- Compute helmet and ski binding points by spatial intersection.
- Compute ski line direction $(\alpha,\beta)$by line intersection.[1]
- Compute "outer" $(\kappa,\varphi_\kappa,\omega_{\kappa,\varphi})_{\text{jumper}}$ and "inner" $(\Psi,\Phi,\Omega)$ performance.
- Compute ski separation and body/ski position.

*Algorithm for 2D measurement and computation*

For i = 1 to $n_{im}$
  Measure $(\boldsymbol{x}_{helm})_i$
  For j = 1,2
    For k = 1 to $(n_{ski})_{i,j}$
      Measure $(\boldsymbol{x}_{ski})_{i,j,k}$
    Next k
    Compute $((a,b)_{ski})_{i,j}$ from measured $(\boldsymbol{x}_{ski})_{i,j,k}$[2]
    Compute $((a,b)_{leg})_{i,j}$ similarly from measured leg points
    Compute intersection $(x_{bind})_{i,j} = (\mathbf{l}_{ski})_{i,j} \cap (\mathbf{l}_{leg})_{i,j}$[3]
  Next j
Next i

*Algorithm for computation of points and lines by spatial intersection*

Compute $\boldsymbol{X}_{helm}$ by intersection of $P_{helm}$ from measured $(\boldsymbol{x}_{helm})_i$, i=1...$n_{im}$
and Eq.(7)
For j = 1,2
  Compute $(\boldsymbol{X}_{bind})_j$ by intersection of $(P_{bind})_j$ from
      computed $(\boldsymbol{x}_{bind})_{i,j}$, i=1...$n_{im}$ and by Eq.(7)

  Compute $(\boldsymbol{q}_{ski})_j$ by Eq.(5a) from measured $((\boldsymbol{x}_{ski})_{i,j,k}$, i=1...$n_{im}$
  and k=1..$(n_{ski})_j$
  Compute $(q_{leg})_j$ similarly
Next j

1. The computation of performance parameters does not depend on position parameters $(\gamma,\delta)$.
2. A simple but less accurate estimation of a 2D line l is to use two line points $p_1$, $p_2$ and consider $\{\mathbf{x}_{p1},\mathbf{x}_{p2}\}\in\mathbf{l}$
3. $\mathbf{x}=[x,y,1]^T$ and $\mathbf{l}=[a,-1,b]^T$

### *3.2 Point and line intersection in space*

This section is based on the following assumptions:

(i) An ideal camera assumed as in Fig. 1 with known pose and principal distance.
(ii) 2D coordinate measurements $(x',y')_p$ of image points p with expectations $(x,y)_p$ and errors $(\varepsilon_x,\varepsilon_y)_p$ given by equations

$$x = x' - \varepsilon_x, \quad y = y' - \varepsilon_y \tag{5}$$

and with standard deviations

$$\sigma_x = \sigma_y (= \sigma_0) \tag{6}$$

with $\sigma_0^2$ as variance factor.

(iii) In the point intersection case, in each image one measured 2D point p corresponding to the actual 3D point P with unknown coordinates (X, Y, Z). In the line intersection case, several points p freely chosen on each image line l corresponding to actual 3D line L with unknown parameters $(\alpha,\beta,\gamma,\delta)$.
(iv) The use of least squares method (LSM) to estimate parameters by the criterion $\sum\left(\hat{\varepsilon}_x^2 + \hat{\varepsilon}_y^2\right) = \min$ with estimated residuals $\left(\hat{\varepsilon}_x, \hat{\varepsilon}_y\right)$ (conf. section 3.1.3 in (Koch, 1999), p. 152).

***Point intersection***

When introducing Eq. (5) into Eq. (1) we get after some reformulation

$$\begin{aligned}\left[\boldsymbol{X} - \boldsymbol{X}_0\right]^T \boldsymbol{r}_3 (x' - \varepsilon_x) &= -c\left[\boldsymbol{X} - \boldsymbol{X}_0\right]^T \boldsymbol{r}_1 \\ \left[\boldsymbol{X} - \boldsymbol{X}_0\right]^T \boldsymbol{r}_3 (y' - \varepsilon_y) &= -c\left[\boldsymbol{X} - \boldsymbol{X}_0\right]^T \boldsymbol{r}_2\end{aligned}$$

with (i) $\boldsymbol{r}_1, \boldsymbol{r}_2, \boldsymbol{r}_3$ corresponding to $\left(\boldsymbol{r}_1, \boldsymbol{r}_2, \boldsymbol{r}_3\right)_{cam}$ in Eq. (2), (ii) stochastic coordinates (x',y'), (iii) errors $(\varepsilon_x,\varepsilon_y)$ and (iv) unknown coordinate vector $\boldsymbol{X} = [X, Y, Z]^T$.

With "derived" errors $(v_x, v_y)$[4] depending on observational errors $(\varepsilon_x,\varepsilon_y)$, and with image index "i" introduced, we get after some further reformulation the "derived" error Eq.s (7a) with weight $w_i$ Eq. (7b) and minimum constraint (7c).

$$\begin{aligned}\left(v_x\right)_i &= -c_i\left[\boldsymbol{X} - \left(\boldsymbol{X}_0\right)_i\right]^T \left(\boldsymbol{r}_1\right)_i - \left[\boldsymbol{X} - \left(\boldsymbol{X}_0\right)_i\right]^T \left(\boldsymbol{r}_3 x'\right)_i, \quad \text{weight } w_i \\ &\text{with } \left(v_x\right)_i = \left[\boldsymbol{X} - \left(\boldsymbol{X}_0\right)_i\right]^T \left(\boldsymbol{r}_3 \varepsilon_x\right)_i\end{aligned} \tag{7a1}$$

$$\begin{aligned}\left(v_y\right)_i &= -c_i\left[\boldsymbol{X} - \left(\boldsymbol{X}_0\right)_i\right]^T \left(\boldsymbol{r}_2\right)_i - \left[\boldsymbol{X} - \left(\boldsymbol{X}_0\right)_i\right]^T \left(\boldsymbol{r}_3 y'\right)_i, \quad \text{weight } w_i \\ &\text{with } \left(v_y\right)_i = \left[\boldsymbol{X} - \left(\boldsymbol{X}_0\right)_i\right]^T \left(\boldsymbol{r}_3 \varepsilon_y\right)_i\end{aligned} \tag{7a2}$$

$$w_i = \left(\left[\boldsymbol{X} - \left(\boldsymbol{X}_0\right)_i\right]^T \left(\boldsymbol{r}_3\right)_i\right)^{-2} \tag{7b}$$

$$\sum_{i=1}^{n_{im}} \left(w\left(\hat{v}_x^2 + \hat{v}_y^2\right)\right)_i = \min \tag{7c}$$

4. In classical error theory, "derived" errors are derived as functions of original observational errors.

The initial run may use $w_i = 1$, later runs $w_i$ updated by Eq. (7b) with solved $\boldsymbol{X}$ from previous run.

*Line intersection in space*

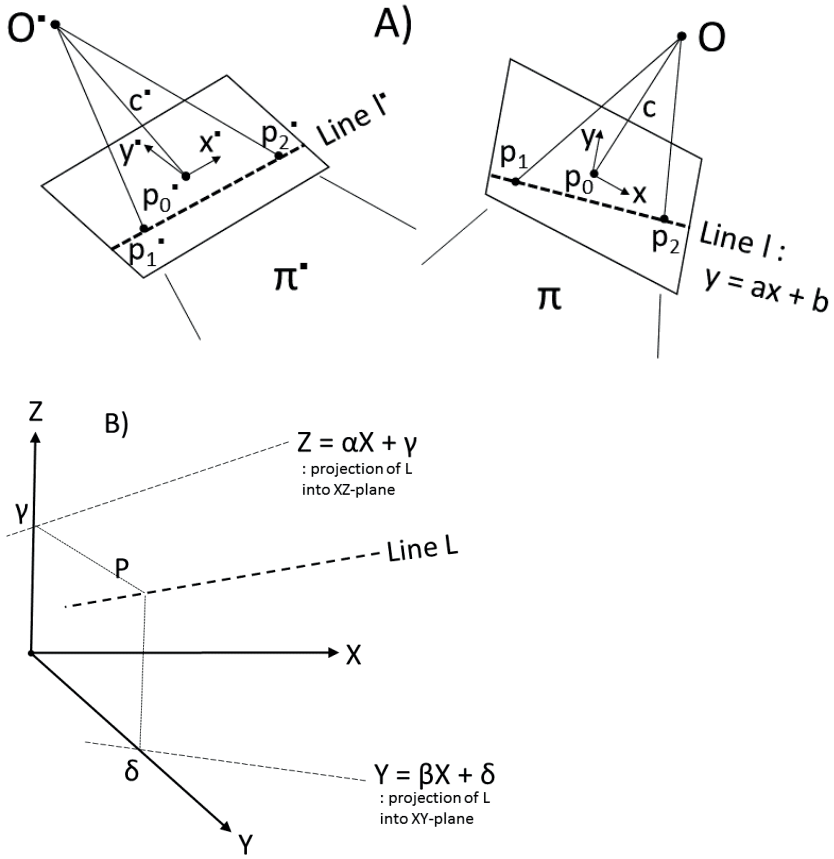


*Figure 3. Geometry of line intersection. Object line L is back-projected as an image line l or l•. A) shows two object planes ($\pi, \pi^{\bullet}$) the intersection of which defines the line L. Plane $\pi$* or *$\pi^{\bullet}$ is defined by projection center O or $O^{\bullet}$ and line l or $l^{\bullet}$. This line is defined by two arbitrary points ($p_1, p_2$) or ($p_1, p_2$)$^{\bullet}$. p0 or p0$^{\bullet}$ is the principle point (origin) in image system (x,y) or (x,y)$^{\bullet}$. B) shows the line L projected as a 2D line in each of planes (XZ) and (XY). Point P represents the penetration of line L in plane (YZ).*

We will present equations and algorithms for an iterative LSM to estimate line parameters $\alpha, \beta, \gamma, \delta$ and their estimation accuracy in one step line intersection based on (indices omitted):

– Coordinate observations $(x', y')$ of freely chosen 2D line points p, Fig. 3-A with errors $(\varepsilon_x, \varepsilon_y)$(Eq. (5) and (6)).
– "Derived" error Eq. (8a) with weight Eq. (8b).
– Minimum constraint (8c).

Eq. (8a) is derived from the 2D line equation in Fig. 3-A by substituting (i) the parameters a and b with their expressions from Eq. (7) and (ii) the coordinates $(x,y)$ considered as expectations of $(x', y')$ by $(x' - \varepsilon_x, y' - \varepsilon_y)$ (conf. Eq. (5)).

With indices reintroduced we get

$$\left\{ v_k = \left[ x'_k, y'_k, -c \right] (\boldsymbol{R}\boldsymbol{u}), \text{weight } w \right\}_i \tag{8a}$$

with $\boldsymbol{R}$ corresponding to Eq. (2), $\boldsymbol{u}$ given by Eq. (4b) and "derived" error $v_k = \boldsymbol{u}^T \boldsymbol{r}_1 \left(\varepsilon_x\right)_k + \boldsymbol{u}^T \boldsymbol{r}_2 \left(\varepsilon_y\right)_k$.

$$\left\{ w = \left( \left( \boldsymbol{u}^T \boldsymbol{r}_1 \right)^2 + \left( \boldsymbol{u}^T \boldsymbol{r}_2 \right)^2 \right)^{-1} \right\}_i \tag{8b}$$

$$\sum_{i,k} w_i \hat{v}_{i,k}^2 = \min \tag{8c}$$

With the right hand side of Eq. (8a) indicated "F," the **Jacobi derivatives** are

$$\frac{\partial F_{i,k}}{\partial \boldsymbol{q}} = \left[ \left( x', y' \right)_k, (-c) \right]_i \boldsymbol{R}_i \frac{\partial \boldsymbol{u}_i}{\partial \boldsymbol{q}} \tag{9}$$

with $\dfrac{\partial \boldsymbol{u}_i}{\partial \boldsymbol{q}} = \begin{bmatrix} \delta - \left(Y_0\right)_i & -\gamma + \left(Z_0\right)_i & \alpha & -\beta \\ \left(X_0\right)_i & 0 & 0 & 1 \\ 0 & -\left(X_0\right)_i & -1 & 0 \end{bmatrix}$

Eq. (8a) is non-linear in unknown $\boldsymbol{q} = \left[\alpha, \beta, \gamma, \delta\right]^T$ via $\boldsymbol{u}$ (conf. Eq (4b)). The iterative LSM needs therefore an approximate, initial $\boldsymbol{q}_0 = \left[\alpha, \beta, \gamma, \delta\right]_0^T$. In case $n_{im} = 2$, $\boldsymbol{q}_0$ is found as parameters of the intersecting line between the projection planes $\pi$ and $\pi'$ (Fig. 3-A). In case $n_{im} > 2$, that image pair is used for this purpose which gives the "best" intersection from singular value decomposition (SVD) (conf. section 12.7 in (Hartley & Zisserman, 2004), p. 321 and appendix C3 in (Nes, et al., 2012)).

The solution process may be formulated as $\boldsymbol{q}_m = \boldsymbol{q}_{m-1} + \Delta\boldsymbol{q}_m, \; m = 1, 2 \ldots$
with $\Delta\boldsymbol{q}_m = \left[\Delta\alpha, \Delta\beta, \Delta\gamma, \Delta\delta\right]_m^T$ solved from the linearized equation with Jacobi derivatives Eq. (9). The first step m = 1 uses $w_k = 1$. Each following step m > 1 uses $w_k$ given by Eq. (8b) with $\boldsymbol{u}_i$ updated by $\boldsymbol{q}_{m-1}$.

The accuracy of solved parameters $(\alpha, \beta, \gamma, \delta)$ is expressed by the variance-covariance matrix $\boldsymbol{N}^{-1}\sigma_0^2$ (conf. section 3.2.2 in (Koch, 1999), p. 160) where $\boldsymbol{N}$ is the coefficient matrix of the normal equations. $\sigma_0^2$ can be estimated as follows.

$\hat{\sigma}_0^2 = \dfrac{\sum_{i=1}^{n_{im}} \sum_{k=1}^{\left(n_p\right)_i} w_i \hat{v}_{i,k}^2}{\left(n_p - 4\right)}$ where $\hat{v}_{i,k}$ are estimated residual deviations in the "derived" error equations (8a) with estimated $(\alpha, \beta, \gamma, \delta)$ inserted, and $n_p = \sum_{i=1}^{n_{im}} \left(n_p\right)_i$ the number of line image points in the images i.

### *3.3 Rotational transformation of lines*

In this section and the following we omit the prefix "jumper" of notations $\boldsymbol{R}$ and angles $(\kappa, \varphi_\kappa, \omega_{\kappa,\varphi})$. Let Eq. (10) express rotational transformation of system (X,Y,Z)to system $\left(\bar{X}, \bar{Y}, \bar{Z}\right)$ with line (L), the direction of which is $(\alpha, \beta)$. In vector form

$$\bar{\boldsymbol{X}} = \boldsymbol{R}\boldsymbol{X} \tag{10}$$

with $\boldsymbol{R}$ as a rotation matrix. Further let Eq.s (11) be the line equations in respective systems $\left(\bar{X}, \bar{Y}, \bar{Z}\right)$ and $\left(X, Y, Z\right)$.

$$\bar{Z} = \bar{\alpha}\bar{X} + \bar{\gamma}, \quad \bar{Y} = \bar{\beta}\bar{X} + \bar{\delta} \tag{11a}$$

$$Z = \alpha X + \gamma, \quad Y = \beta X + \delta \tag{11b}$$

From Eqs. (10) and (11) we may derive Eqs. (12) expressing $\left(\bar{\alpha}, \bar{\beta}\right)$ as a function of $\left(\alpha, \beta\right)$ where $\boldsymbol{R}^{\mathrm{T}} = \left[\boldsymbol{r}_1, \boldsymbol{r}_2, \boldsymbol{r}_3\right]$.

$$\bar{\alpha} = \frac{(\boldsymbol{r}_3)^{\mathrm{T}}\left[1, \beta, \alpha\right]^{\mathrm{T}}}{(\boldsymbol{r}_1)^{\mathrm{T}}\left[1, \beta, \alpha\right]^{\mathrm{T}}} \tag{12a}$$

$$\bar{\beta} = \frac{(\boldsymbol{r}_2)^{\mathrm{T}}\left[1, \beta, \alpha\right]^{\mathrm{T}}}{(\boldsymbol{r}_1)^{\mathrm{T}}\left[1, \beta, \alpha\right]^{\mathrm{T}}} \tag{12b}$$

Section 4.5.4 in (Luhmann, et al., 2006) contains the derivation of corresponding equations (Eq. 4.143) under somewhat different assumptions of coordinate systems.

### *3.4 Solving the performance parameters*

This section solves the "outer" parameters (direction, forward slope and sideway slope) as well as "inner" parameters (Boklöv, scissor and closing angles). Finally, the ski separation and model position in the hill system are considered.

#### Direction κ and forward slope $\varphi_\kappa$

Based on Eq. (3b) and Eq. (12b) where $\left(\alpha, \beta, \bar{\beta}, \boldsymbol{R}\right)$ are replaced by $\left((\alpha,\beta)_{\mathrm{mid}}, (\beta_{\mathrm{mid}})_\kappa = 0, \boldsymbol{R}_\kappa\right)$ we find Eq. (13a). Substituting the elements of $\boldsymbol{R}_\kappa$ by their κ-functions corresponding to Eq. (2) we get κ given by Eq. (13b).

$$\beta_{\mathrm{mid}} = \left(\frac{r_{12}}{r_{11}}\right)_\kappa \tag{13a}$$

$$\tan\kappa = \beta_{\mathrm{mid}} \tag{13b}$$

Based on Eq. (3a) and Eq. (12a) where $\left(\alpha, \beta, \bar{\alpha}, \boldsymbol{R}\right)$ are replaced by $\left((\alpha,\beta)_{\mathrm{mid}}, (\alpha_{\mathrm{mid}})_{\kappa\varphi} = 0, \boldsymbol{R}_{\kappa\varphi}\right)$ we find Eq. (14a). Substituting elements of $\boldsymbol{R}_{\kappa\varphi}$ by κφ-functions corresponding to Eq. (2) we get $\varphi_\kappa$ given by Eq. (14b).

$$\alpha_{\mathrm{mid}} = \left(\frac{r_{13}}{r_{11}}\right)_{\kappa,\varphi} \tag{14a}$$

$$\tan \varphi_{\kappa} = \alpha_{mid} \cos \kappa \tag{14b}$$

**Sideway slope $\omega_{\kappa\varphi}$ and closing angle Ω**

$\omega_{\kappa\varphi}$ is found by a ω-rotation about a rotated X-axis giving Eq. (15) under constraint $P_{helm} \in (XZ\text{-plane})_{\kappa,\varphi,\omega}$, giving Eq. (16).

$$\left(\boldsymbol{X}_{\kappa,\varphi,\omega}\right)_{helm} = \boldsymbol{R}_{\omega}\left(\boldsymbol{X}_{\kappa,\varphi}\right)_{helm} \tag{15}$$

$$\left(Y_{\kappa,\varphi,\omega}\right)_{helm} = 0 \tag{16}$$

From Eqs. (15) and (16) we may derive Eq. (17) by which $\omega_{\kappa,\varphi}$ is given

$$\tan \omega_{\kappa,\varphi} = \left(\frac{Z_{helm} - Z_{mid}}{Y_{helm} - Y_{mid}}\right)_{\kappa,\varphi} \tag{17}$$

with $(Y,Z)_{mid}$ given by Eq. (21).

Ω is computed by equation (see Fig. 1):

$$\tan \Omega = \frac{Z_{helm} - Z_{mid}}{X_{helm} - X_{mid}} \tag{18}$$

**Boklöv angle Ψ and scissor angle Φ**

Ψ is computed by the equation:

$$\Psi = \left|\tan^{-1}\left(\beta_{ski}\right)_1\right| + \left|\tan^{-1}\left(\beta_{ski}\right)_2\right| \tag{19}$$

with $(\beta_{ski})_j$ obtained by ski line intersection.

ϕ is computed by the equation:

$$\phi = \left|\tan^{-1}\left(\alpha_{ski}\right)_1\right| + \left|\tan^{-1}\left(\alpha_{ski}\right)_2\right| \tag{20}$$

with $(\alpha_{ski})_j$ obtained by ski line intersection.

**Position and ski separation**

The position $\boldsymbol{X}_{mid}$ of point $P_{mid}$ defining the **position of the body/ski model** is computed by the equation:

$$\boldsymbol{X}_{mid} = \frac{\left(\boldsymbol{X}_{bind}\right)_1 + \left(\boldsymbol{X}_{bind}\right)_2}{2} \tag{21}$$

with $(\boldsymbol{X}_{bind})_j$ as the positions of the spatially intersected ski binding points $(P_{bind})_j$.

**Ski separation i** s defined as the Euclidean distance between ski binding points $(P_{bind})_j$ and is computed by the equation:

$$s = d\left(\left(P_{bind}\right)_1, \left(P_{bind}\right)_2\right) \tag{22}$$

## 4 Simulated example estimating the inner parameters Boklöv, scissor and closing angles

The example approximates a stereo pair just after takeoff in a test jump in Granåsen ski jump arena (Nes, et al., 2012) as to (i) camera position and rotation ("pose"), (ii) skis and body modelled as straight lines and (iii) helmet modelled as a recognizable, natural target point. Thus, the algorithm to compute the Boklöv, scissor and closing angles may be as follows (see also Fig. 4):

- Simulate (i) arbitrarily chosen 3D points (P) 1, 2, 3, 4 on ski lines and 5, 6 on leg lines, (ii) helmet point ($P_{helm}$) lying on $(L_{leg})_1$ and $(L_{leg})_2$ and (iii) poses of two ideal cameras (section 2.4). All of these refer to a system (X, Y, Z) in which (a) the rotation performance parameters $\kappa$, $\phi_\kappa$, $\omega_{\kappa\phi}$ (section 2) are equal to 0, and (b) the origin is defined as in Fig. 2.
- In the two images, compute by Eq. (1) the corresponding image points (p) 1, 2, 3, 4, 5, 6 and $(p_{helm})_j$, all considered as having stochastic observed 2D coordinates (see Eqs. (5),(6)) with image points 1, 2, 3, 4 on 2D ski lines and image points 5, 6 $(p_{helm})_j$ on 2D leg lines. Note that points 1 to 6 are considered as arbitrarily chosen in the images, not necessarily corresponding over the images.
- Compute via the spatial intersection of ski lines the **Boklöv** and **scissor angles** by the formula given in section 3.4.
- Considering 2D helmet points $(p_{helm})_j$ as observational points corresponding over the image, compute via the intersection of helmet point ($P_{helm}$), the **closing angle** by Eq. (18) in section 3.4.

**Results** (with $\sigma_0$ guessed 0.4 pixels (see Eqs. (5), (6))
Boklöv-angle = 14° ($\sigma$ = 4.0°)
Scissor-angle = 11° ($\sigma$ = 0.14°)
Closing-angle = 45° ($\sigma$ = 0.10°)

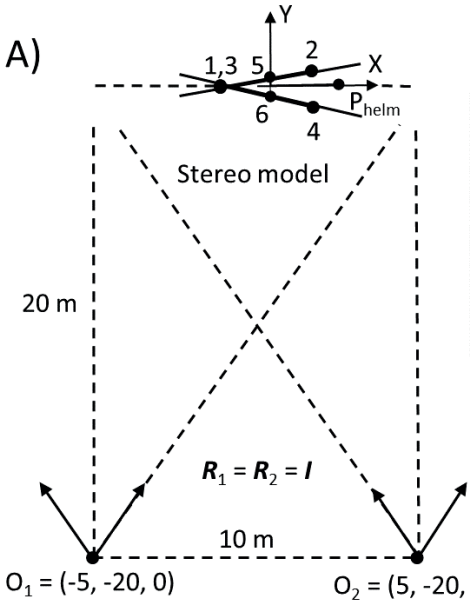


| | X | Y | Z |
|---|---|---|---|
| 1 | -1 | 0 | -0.1 |
| 2 | 1 | 0.25 | 0.1 |
| 3 | -1 | 0 | 0.1 |
| 4 | 1 | -0.25 | -0.1 |
| 5 | 0 | 0.125 | 0 |
| 6 | 0 | -0.125 | 0 |
| helm | 1.2 | 0 | 1.2 |

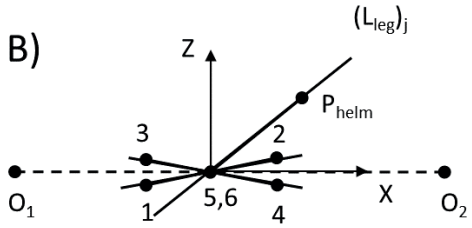


*Figure 4. Geometry with object points and camera poses simulated. A) is the projection in the XY-plane and B) is the projection in the XZ-plane. The origin is equal to the midpoint of* $(P_{bind})_j$. *Points 5 and 6 are placed near* $(P_{bind})_j$.

In the simulated examples of (Ryu, et al., 2015) , a ski jumper with closing angle $\Omega = 10° – 30°$ and Boklöv angle $\Psi = 0 – 35°$ is chosen based on a reference jump. In our simulated example, a closing angle is chosen $\Omega = 45°$ and a Boklöv angle is chosen $\Psi = 14°$. The Boklöv angle is in the same range and closing angle is larger than in Ryu et al. (2015) since our example considers early flight phase just after takeoff.

## 5 Summary, discussion and further work

This article deals with markerless estimation of a ski jumper's performance parameters, i.e., without established, predefined markers on the body/skis. In comparison with marker-based estimation, the markerless approach involves particular operations not so common in traditional photogrammetry. These may cause lower accuracy and reliability if not properly attended to in the network design. We first define the body/ski model used, then summarize and discuss some highlights of the markerless operations, including an overview of parameter definitions. We conclude with a discussion of possible further research on the markerless approach.

### *The body/ski model*

We have assumed a somewhat oversimplified model with (i) straight ski and leg lines, (ii) a natural helmet point and (iii) ski binding points corresponding to image points intersected by 2D leg and ski lines. A model coordinate system $(X, Y, Z)_{jumper}$ is constructed by sequential $\kappa$-, $\varphi$-, $\omega$ -rotations about moveable axes Z, Y and X, respectively, in the hill system (X, Y, Z).

### *Numerical operations*

The first operation described in section 3.3 computes (i) ski and leg lines (parameters $\alpha$, $\beta$, $\gamma$, $\delta$) and (ii) helmet and ski binding points (coordinates X, Y, Z), by respective line and point intersections in space. Section 3.4 then shows the final computation of relevant performance parameters in accordance with assumed parameter definitions.

### *Parameter definitions*

Direction and forward slope are the respective angles $\kappa$ and $\varphi_\kappa$ that rotate the hill system (X, Y, Z) with movable axis: $\kappa$ about Z and $\varphi_\kappa$ about $\kappa$-rotated Y, making the $\kappa$,-rotated X-axis parallel with the $\kappa$,$\varphi$-rotated midline $L_{mid}$ ($L_{mid}$ is the mean of the two ski lines, Fig. 2). Sideway slope is the angle $\omega_{\kappa,\varphi}$ obtained by $\omega$-rotation about the $\kappa$,$\varphi$-rotated X-axis, making the helmet point $P_{helm}$ lie on the YZ-plane of system $(X, Y, Z)_{jumper}$ (see Fig. 2).

Closing angle ($\Omega$), Boklöv angle ($\Psi$) and scissor angle ($\Phi$) may be geometrically defined as shown in Fig. 2. Body/ski position is the position of the midpoint between the ski binding points.

### *Precision and reliability of estimated performance parameters*

It should be noted that intersection of points and lines assuming "constant" camera poses may give an overly optimistic evaluation of the accuracy of estimated performance parameters. The commonly used approach to accuracy evaluation is either to use the somewhat time consuming Monte Carlo simulation (Hastedt, 2004) or to use the law of propagation of cofactors (Koch, 1999). In the simulated example in Section 4, the latter approach is used to evaluate the accuracy of the LSM estimated Boklöv angle, scissor angle and closing angle.

Noticing that the hill system, defined as in Section 2, is approximately parallel to the $(X,Y,Z)_{jumper}$ system, the precision of the angular performance parameters in an image pair situation is made optimal by:

- Reasonably small direction parameters $(\alpha,\beta)$ defined by Fig. 3-B (Schwermann, 1995). In the Granåsen project the ski direction $(\alpha,\beta) <$ ca. 45° (Nes, et al., 2012).

- A small slope 'a' of the image line defined by Fig. 3-A.
- Avoiding body/ski lines nearly parallel with the base line or lying near the epipolar plane.

The possibility of ill-conditioning or singularity caused by improperly planned camera positions is demonstrated by a simulated example in Section 4.

Compared to estimating body/ski lines from marker-based point intersection, markerless line intersection is more flexible and independent of the viewing direction, facilitating use of cameras placed on both sides of the jumping field.

**Future research**

Further research should focus on topics like:

(i) Application of a more exact modelling of body/skis, for instance using non-straight-line features (see section 4.5.6 in (Luhmann, et al., 2006), p. 301).
(ii) Digital feature recognition and automatic (x,y) measurement.
(iii) Integration of both line and point features (unknown or known) in a one-step phototriangulation, implying autocalibration of the interior and exterior orientation.
(iv) Use of the Hough transform to recognize both straight and curved body/ski lines.

We also offer some further thoughts on future automatic feature detection in video images. In practical cases, for instance images from Granåsen, the ski jumper can be found from the segmented images using temporal median filtering, a form of background subtraction described in (Piccardi, 2004). This segmentation results in greyscale images in which non-moving image features are removed and features of a moving ski jumper are preserved. The most significant lines in the images represent the skies, which can be found using the Hough transformation (Duda & Hart, 1972). If the resolution is high, such that the ski width covers several pixels, one can use edge detection combined with mathematical morphology and thinning algorithms to represent skis as lines. Another issue concerns whether bending skis during takeoff may be modelled as curved lines. In such cases the Hough transform can be converted to handle curved image lines $y = ax^2 + bx + c$. Further, the ski jumper helmet can be found from the same background-subtracted images. A general approach should be developed where one takes into account the orientations of the cameras as well as varying orientations of the ski jumper.

**References**

Duda, R.O. & Hart, P.E., 1972. Use of the Hough transformation to detect lines and curves in pictures. *Communications of ACM,* 15(1), pp. 11–15.

Hartley, R. & Zisserman, A., 2004. *Multiple View Geometry in Computer Vision.* 2nd ed. Cambridge: Cambridge University Press.

Hastedt, H., 2004. *Monte-Carlo-Simulation in Close-Range Photogrammetry.* Istanbul, Turkey, The International Archives of the Photogrammetry, Remote Sensing and Spatial Information Science, pp. 18–23.

Jung, A., Staat, M. & Müller, W., 2015. *Effect of wind on flight style optimisation in ski jumping.* Edinburgh, UK, s.n.

Koch, K.-R., 1999. *Parameter Estimation and Hypothesis Testing in Linear Models.* 2nd ed. s.l.:Springer.

Luhmann, T., Robson, S., Kyle, S. & Harley, I., 2006. *Close Range Photogrammetry: Principles, Techniques and Applications.* s.l.:Whittles Publishing.

McGlone, J.C. ed., 2004. *Manual of Photogrammetry.* 5th ed. s.l.:asprs.

Nes, A., Hådem, I. & Nilsen, J.H., 2012. Capturing the motion of ski jumpers using multiple stationary video cameras. *Kart og plan,* 105(1), pp. 56–80.

Piccardi, M., 2004. *Background subtraction techniques: a review.* s.l., s.n., pp. 3099–3104.

Poppe, R., 2007. Vision-based human motion analysis: An overview. *Computer vision and image understanding,* 108(1), pp. 4–18.

Ryu, M., Cho, L. & Cho, J., 2015. Aerodynamic Analysis on Postures of Ski Jumpers during Flight using Computational Fluid Dynamics. *Transactions of The Japan Society for Aeronautical and Space Sciences,* 58(4), pp. 204–212.

Schwameder, H., 2008. Biomechanics research in ski jumping 1991–2006. *Sports Biomechanics,* 7(1), pp. 114–136.

Schwameder, H. et al., 2005. Kinematic characteristics of the early flight in ski-jumping. *Science and skiing III,* pp. 381–391.

Schwermann, R., 1995. *Geradengestützte Bildorientierung in der Nahbereichsphotogrammetrie,* Aachen: s.n.

Virmavirta, M. et al., 2005. Characteristics of the early flight phase in the Olympic ski jumping competition. *Journal of Biomechanics,* 38(11), pp. 2157–2163.